# Enhanced processing in arrays of optimally tuned nonlinear biomimetic sensors: A coupling-mediated Ringelmann effect and its dynamical mitigation

Alexander P. Nikitin,[1,*] Adi R. Bulsara,[2,†] and Nigel G. Stocks[1,‡]

[1]*School of Engineering, University of Warwick, Coventry CV4 7AL, United Kingdom*
[2]*Space and Naval Warfare Systems Center Pacific, Code 71000, San Diego, California 92152-6147, USA*

Inspired by recent results on self-tunability in the outer hair cells of the mammalian cochlea, we describe an array of magnetic sensors where each individual sensor can self-tune to an optimal operating regime. The self-tuning gives the array its "biomimetic" features. We show that the overall performance of the array can, as expected, be improved by increasing the number of sensors but, however, coupling between sensors reduces the overall performance even though the individual sensors in the system could see an improvement. We quantify the similarity of this phenomenon to the Ringelmann effect that was formulated 103 years ago to account for productivity losses in human and animal groups. We propose a global feedback scheme that can be used to greatly mitigate the performance degradation that would, normally, stem from the Ringelmann effect.

## I. INTRODUCTION

Biological sensory systems are remarkable in their ability to detect extremely weak signals. As examples, the human eye is able to count single photons [1], hair cells in the cat cochlea are able to detect displacements of the basilar membrane smaller than $10^{-10}$ m [1], the olfactory system of the domesticated silk moth (*Bombyx mori*) can detect single molecules of pheromone [2], and thermal receptors in crotalid snakes are able to recognize the temperature difference of $0.003\,^\circ$C [3]. All these systems share a simple design principle based on sensor array architectures; high sensitivity is achieved through the use of a large number of sensory receptors.

If the signals are discrete (photons and molecules), large numbers of receptors are necessary to increase the probability of a detection event. If the signals are continuous, e.g., acoustic stimuli, large numbers of receptors are known to work in parallel to reduce the system noise and enhance fidelity. In all the above-mentioned cases, the system sensitivity is proportional to the number of receptors. A specific example of the extreme sensitivity in biological sensory systems is afforded by owls. In the frequency range 5–10 kHz, owls demonstrate better sensitivity to weak acoustic signals than other birds and mammals [4]. This frequency range corresponds to one octave. But the mechanoreceptors tuned to this frequency range cover almost half the length of the basilar papilla (the hearing organ which contains the mechanoreceptors), i.e., 6 mm/octave [5]; this is greater than the values reported for other birds (0.35–1 mm), and mammals (1–4 mm) [6,7]. This example shows that the high concentration (in the frequency domain) of the mechanoreceptors leads to both the exceptional sensitivity to weak acoustic signals and the high frequency resolution.

Another key design principle of biological sensory systems is adaptability. Biological systems typically tune their internal parameters to accommodate changes in the signal strength.

Such adaptation, similar to automatic gain control, not only increases the dynamic range but also protects sensitive systems to damage from large signals. Two well known examples are the mammalian ear, which has a dynamic range of 120 dB but can also detect sound intensities of less than 1 pW/m², and the human eye, which can register single photon detection but has a luminesence range of $10^{14}$. These remarkable features of biological sensory systems have motivated scientists and engineers to adopt a "biomimetic" approach for the design of advanced sensory systems [8–10]. We describe such an approach in this paper, utilizing sensor adaptation in conjunction with array processing to improve the performance of a system based on fluxgate magnetometers.

Specifically, we study Takeuchi and Harada (TH) magnetic sensors assembled into an array; the aim is to increase the total array gain and improve the (total) output signal-to-noise ratio (SNR) over a wide dynamic range. The magnetic sensor invented by Takeuchi and Harada is a simple and small system [11], it displays very good sensitivity to weak magnetic fields because it employs positive magnetic feedback resulting in oscillatory instability; the instability can be exploited to enhance sensitivity. We modify the TH sensor to include a self-tuning mechanism inspired by nonlinear dynamical features of the auditory system of animals; this biomimetic sensor can achieve a large dynamic range, with a concomitant lower noise floor, via adaptation to input signals.

The TH magnetic sensors are, of course, detectors of the target (usually at dc or extreme low frequency) magnetic field; however, they also interact (electromagnetically) with each other when they are placed in an array. This interelement coupling is unavoidable and turns out to be an important and interesting feature of the array, with analogies to work on coupled systems carried out by Ringelmann, an agricultural engineer, over 100 years ago.

The paper is structured as follows. We start by presenting a phenomenological model of the TH magnetic field sensor [11]; this is our "test bed" throughout this paper. We then develop the sensor model further by adding a self-tuning mechanism that biases the sensor into an optimal operating regime, in a single (i.e., uncoupled) sensor. The self-tuning is inspired by the adaptive amplification mechanism that is mediated by

*a.nikitin@warwick.ac.uk
†bulsara@spawar.navy.mil
‡n.g.stocks@warwick.ac.uk

hair cells in the cochlea [12]. The next step is to introduce an array of coupled identical TH elements, together with the phenomenological (including the self-tuning mechanism) dynamics for each element in the array. We quantify the degradation (stemming from the coupling) of the output SNR, and compare this with a well-known (in the social sciences literature) effect first studied by Ringelmann some 103 years ago [13].

In his studies, Ringelmann focused on the maximum performance of human groups (he also studied the performance of teams of oxen yoked to a plough) involved in experiments wherein they used different methods to push or pull a load horizontally [13]. Ringelmann showed that the maximal "productivity" ($P$) of a group (of size $N$) is less than the expected value that would, nominally, be the sum of the maximal productivities of the group members performing alone:

$$P_{\text{group}} < P_{\text{expected}} \equiv \sum_{i=1}^{N} P_{i,\text{alone}}, \quad i = 1 \ldots N. \quad (1)$$

Equation (1) encapsulates the essence of the Ringelmann effect (RE). We provide a more detailed description of the RE later in this paper, when we demonstrate that the coupling-mediated losses in our array bear a striking resemblance to phenomena studied 103 years ago by Ringelmann; we speculate that the origin of this common behavior is almost certainly due to similar coupling effects in Ringelmann's original studies.

Finally, we introduce a possible route for mitigating performance degradation in the array by using a carefully defined global feedback in the sensor array to (partially) cancel the loss terms that stem from the interelement coupling. This "correction" has the effect of raising the output SNR (of the array) to a value close to (but *not* in excess of) the theoretical maximum response SNR; the latter limit is calculated as the sum of the response SNRs of individual elements in the array, assuming zero interelement coupling. We conjecture that, at least in the cochlea, this type of feedback should be present to mitigate Ringelmann-type losses.

## II. MODEL

### A. Magnetic field sensor of Takeuchi and Harada

The sensor circuit is shown in Fig. 1(a) [11]. We see that the sensor is a combination of an oscillator through the $L_0 C_0$ resonance circuit, and a low-pass filter $R_2 C_2$.

In the resonance circuit, the inductance $L_0$ is nonlinear due to a ferromagnetic core. The power loss in the resonance circuit occurs due to the resistance of the coil and hysteresis in the ferromagnetic core. For self-sustained oscillations, the power loss in the resonance circuit should be compensated by a positive feedback. In the sensor of Takeuchi and Harada (TH), the positive feedback is implemented with the resistance $R_1$, and the inductance $L_1$; the operational amplifier is used as a comparator.

In the oscillating magnetic field of the resonance circuit, the ferromagnetic core is periodically saturated. If an external constant magnetic field is applied, the oscillations in the sensor output take on an asymmetric form due to the nonlinearity of the ferromagnetic core. Hence the oscillator output averaged
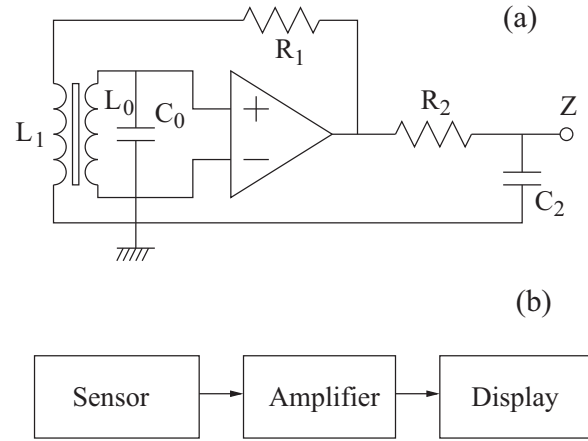


FIG. 1. (a) Circuit of Takeuchi and Harada. (b) The complete measuring system.

by the low-pass filter $R_1 C_1$ is different from zero in this case. Here, it is assumed that the oscillations are fully filtered out by the low-pass filter.

The transfer function of the sensor is not monotonic [11]. Here, we introduce a phenomenological model of the transfer function to simplify our task of analysis of the noisy nonlinear system. We do not seek a precise quantitative agreement between our model and the experimental results (see Fig. 2 in this manuscript and Fig. 3 in Ref. [11]); rather, we need a qualitative agreement only. This simplification has been carried out precisely to make it possible to explain the RE in an array of TH sensors locked by their adaptation feedbacks. Hence we avoid a situation wherein we might be overwhelmed with a plethora of details and parameters of the complex system; these details are, as stated above, unimportant to our stated goal of exploring the RE in an array of these sensors.

The transfer function can be, qualitatively, described by the following equation:

$$f(x,q) = \text{sgn}(x)\sqrt{q}\left[1 - \exp\left(-\frac{|x|}{q}\right)\right]\exp\left(-\frac{x^2}{q^2}\right), \quad (2)$$
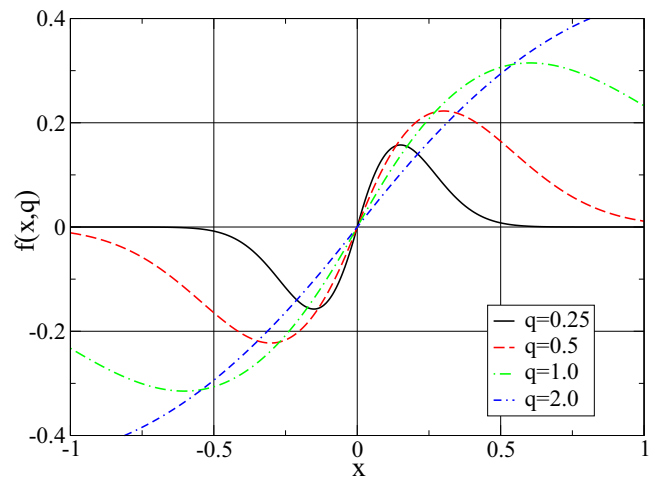


FIG. 2. Transfer function of the model for a set of parameters: $q = 0.25$, $q = 0.5$, $q = 1.0$, and $q = 2.0$.
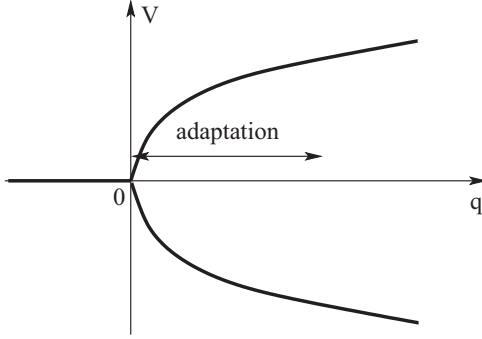
FIG. 3. Bifurcation diagram of the Takeuchi and Harada sensor (shown schematically). The parameter $V$ represents the amplitude of the voltage oscillations in the $L_0 C_0$ resonance circuit. The parameter $q$ depends on $R_1$. $q = 0$ corresponds to the Hopf bifurcation.

where $x$ is an applied magnetic field, and $q$ is a parameter characterizing the feedback of the oscillator. It is assumed that $0 \leqslant q < \infty$. Then, the closer the parameter $q$ is to zero, the smaller is the excitation of the resonance circuit via the feedback. The case $q = 0$ corresponds to the Andronov-Hopf bifurcation in the TH oscillator (see Fig. 3). We note here that Eq. (2) is, however, not able to describe the Andronov-Hopf bifurcation itself.

The sensor can be characterized by the maximal value of the coefficient of amplification, and the dynamic range. According to Eq. (2), the coefficient of amplification of the sensor is $k_q = f(x,q)/x$. The maximal value of the coefficient of amplification can be found, in the limit $x \to 0$, as $k_{q,\max} = 1/\sqrt{q}$. In practice, sensors are usually exploited in a range of inputs wherein their transfer functions are almost linear functions of the (small) input signals. Therefore, the dynamic range of the sensor can be defined as the range of $x$ where the transfer function $f(x,q)$ deviates from the linear function $F(x,q) = k_{q,\max} x$ up to a small parameter $\delta$,

$$|F(x,q) - f(x,q)| < \delta, \quad \delta > 0.$$

Since $\delta$ is small, the transfer function can be well approximated by the cubic equation

$$f(x,q) \simeq ax^3 + bx^2 + cx + d.$$

From the symmetry of the transfer function $f(x,q) = -f(-x,q)$, it follows that $b = 0 = d$. In the limit of small values of $x$, the transfer function becomes almost linear $f(x,q) \simeq cx$, so that $c = k_{q,\max}$. Therefore,

$$|F(x,q) - f(x,q)| \simeq |ax^3|,$$

just outside the linear regime of the transfer function. A Taylor expansion (about the origin) of Eq. (2) yields $a \simeq -q^{-5/2}$; hence the dynamic range of $x$ is $[-\delta^{1/3} q^{5/6} : \delta^{1/3} q^{5/6}]$. One readily observes that (i) the parameter $q$ controls both the dynamic range and the coefficient of amplification and (ii) the dynamic range narrows faster than the amplification coefficient increases.

From this brief analysis it follows that it is possible to reach very high values of the coefficient of amplification (i.e., high sensitivity to weak signals) close to the limit $q \to 0$, precisely where there is a risk of failure in the sensor operation due it

being poised on the brink of the Andronov-Hopf bifurcation. In this limit, however, the internal noise plays a very important role in the sensor dynamics because it is amplified by the sensor either instead of or with the target signal. In the output of the TH sensor, the noise $\xi(t)$ is colored (i.e., correlated with correlation time $\tau_\xi$) because it is passed via a low-pass filter of first order with large time constant. Previously, we had introduced the noninertial and noise-less transfer function Eq. (2). Therefore, to describe the noise dynamics of the sensor we must assume that noise is present at the input of our model, $x = s + \xi(t)$, where $s$ is a target dc magnetic field. The noise can be represented by the Ornstein-Uhlenbeck (OU) process,

$$\tau_\xi \frac{d\xi}{dt} = -\xi + \sqrt{2D}\eta(t), \tag{3}$$

with correlation function

$$\langle \xi(t_1)\xi(t_2) \rangle = \sigma_\xi^2 \exp\left(-\frac{|t_1 - t_2|}{\tau_\xi}\right),$$

where $\tau_\xi$ and $\sigma_\xi^2 = D/\tau_\xi$ are the correlation time and the variance of the OU process correspondingly; $\eta(t)$ is a Gaussian white noise with zero mean $\langle \eta(t) \rangle = 0$ and correlation function $\langle \eta(t_1)\eta(t_2) \rangle = \delta(t_1 - t_2)$, with $2D$ being the noise intensity. For practical applications, the input values $(s + \xi(t))$ should be set up inside the dynamic range of $x$. Therefore, the relationship between the noise level and the dynamic range should be $\sigma_\xi < \delta^{1/3} q^{5/6}$ or, for simplicity, $\sigma_\xi < \delta^{1/3} q$. Hence the coefficient of amplification must be bounded from above as $k_{q,\max}^2 < \delta^{1/3}/\sigma_\xi$.

If the target magnetic field $s$ is too weak or too strong, the sensor output could be out of the dynamic range of the display or another readout device. Therefore, we need an amplifier or an attenuator to complete the measurement system [see Fig. 1(b)]. In the case of a weak output of the sensor, when its value is comparable with the input noise of the amplifier, the amplifier will amplify both the output of the sensor and its own internal noise,

$$v = k_a(f(s + \xi, q) + \xi_a),$$

where $k_a$ is the coefficient of amplification of the amplifier, $v$ its output, and $\xi_a$ the input noise of the amplifier. With the assumption $f(x,q) \simeq k_q(x + \xi)$, we obtain

$$v = k_a(k_q s + k_q \xi + \xi_a). \tag{4}$$

Now, it is easy to obtain the output signal-to-noise ratio,

$$\Gamma_{\text{out}} = \frac{\langle v \rangle^2}{\sigma_v^2} = \frac{s^2}{\sigma_\xi^2 + \sigma_{\xi_a}^2/k_q^2}. \tag{5}$$

Here $\langle v \rangle$ is the mean value of the output; $\sigma_v^2$ and $\sigma_{\xi_a}^2$ are the variances of the output and noise of the amplifier correspondingly.

The last equation shows the output SNR to be monotonically decreasing with increasing $k_q$. In the limit of very high $k_q$, the SNR at the output of the measurement system approaches the SNR at the input of the sensor. Therefore, to improve the SNR of the complete measurement system we need to increase the coefficient of amplification of the sensor, $k_q$, as much as possible.

## B. Biomimeticity: The self-tuning mechanism

It is well known that, in the auditory system, a self-tuning mechanism allows an adaptation of the dynamical range of the system to different levels of input signals [12]. In the absence of input signals the system will increase its coefficient of amplification until the amplified internal noise in the output reaches a significant level. If a signal is then applied, both the signal and noise are amplified together so that the total output power is increased but to a small level compared with the signal-less condition. The system is organized so that the strongest signal is amplified with the smallest amplification coefficient [12].

We introduce a self-tuning mechanism with similar properties for our realization of the TH sensor. For signal and noise inside the dynamic (working) range, the output power of the sensor can be estimated as

$$\hat{\psi} = \langle [f(s + \xi(t),q)]^2 \rangle.$$

In this equation we have tacitly assumed the existence of an ensemble of sensors so we can use the ergodic hypothesis for an estimation of the (average) power. Moreover, we replace the infinite interval of time (over which the averaging is done) with a finite interval $T$,

$$T \frac{d\psi}{dt} = -\psi + [f(s + \xi, q)]^2. \tag{6}$$

For sufficiently large $T$, this provides a good estimator of the power, $\hat{\psi} \simeq \psi$.

To use the entire dynamic range of the sensor, the power provided by the input signal should be close or equal to the boundary of the dynamic range of the sensor, $\langle x^2 \rangle = [\delta^{1/3} q^{5/6}]^2 \simeq \delta^{2/3} q^2$. In this case, taking into account the quasilinear character of the function $f(x,q)$ in the dynamic range, the power of the output can be estimated as $\tilde{\psi} = [f(\sqrt{\langle x^2 \rangle}, q)]^2 = [f(\sqrt[3]{\delta}\, q, q)]^2 \simeq [k_{q,\max} \delta^{1/3} q]^2 = q\, \delta^{2/3}$. Hence the value of the parameter $q = \psi\, \delta^{-2/3}$ indicates an optimal usage of the dynamic range of the sensor. Now, the self-tuning mechanism for our model of the sensor can be described by the equation

$$\tau \frac{dq}{dt} = -q + \psi\, \delta^{-2/3}, \tag{7}$$

where $\tau$ is the tuning time. It is assumed that the tuning time $\tau$ is equal to or greater than the averaging time $T$, i.e., $\tau \geqslant T$. Equations (2), (3), (6), and (7) are the model of the sensor with the tuning mechanism.

Figure 4 schematically shows a possible setup of the adaptive system: the input $x$ is transformed into the output $z$ that is passed via a nonlinear unit (to obtain $z^2$) and a linear low pass filter to control the parameter $q$ in the transfer
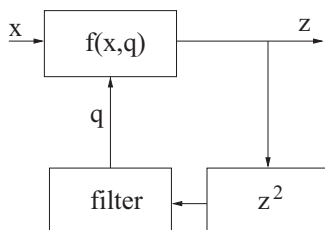
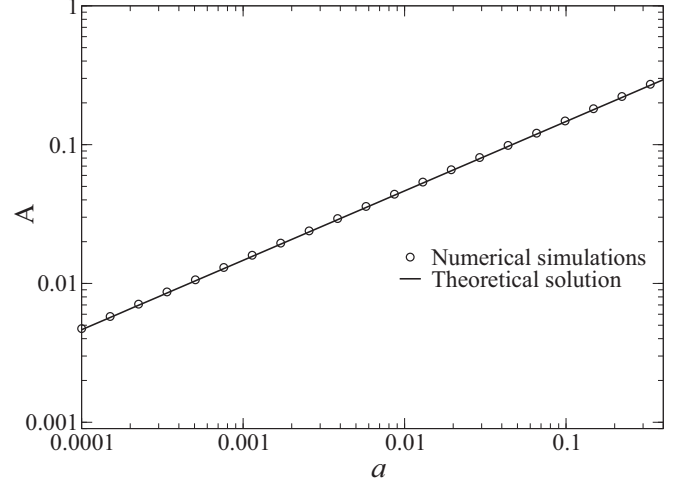FIG. 4. Possible setup of the adaptive system.

FIG. 5. Input-output characteristics of the adaptive system. The periodic input signal is $x = a \cos \Omega t$. $A$ is the amplitude of the main harmonic in the output. It is found as $A = \sqrt{A_1^2 + B_1^2}$, where $A_1 = \frac{1}{\pi/\Omega} \int_0^{2\pi/\Omega} z \cos(\Omega t) dt$ and $B_1 = \frac{1}{\pi/\Omega} \int_0^{2\pi/\Omega} z \sin(\Omega t) dt$ via simulations of Eqs. (2), (3), (6), and (7). Parameters: $\Omega = 2\pi \times 0.01$, $\delta = 0.01$, and $T = \tau = 10$. The theoretical solution was obtained with Eq. (8).

function $f(x,q)$. The Hopf bifurcation and the adaptation regime for the TH sensor are schematized in Fig. 3. In Fig. 5 the input-output characteristic of the adaptive system is shown. The so-called "compression" [12] is readily visible: weak signals are amplified but strong signals are attenuated. In the interest of completeness, we evaluate the transfer function of the sensor using a linear approximation. We start by replacing the true $\psi$ with its estimate $\overline{[f(x,q)]^2}$. Then, by assumption, the parameter $q$ is stationary and can we rewrite Eq. (7),

$$q = \overline{[f(x,q)]^2} \delta^{-2/3}.$$

Next, we substitute the linear approximation $f(x,q) \simeq x/\sqrt{q}$ into the previous equation to obtain

$$q = \frac{\delta^{-2/3}}{q} \overline{x^2}.$$

This, immediately, leads to

$$q = \delta^{-1/3} \sqrt{\overline{x^2}},$$

whence the transfer function is obtained as

$$z = f(x,q) \simeq \frac{x}{\sqrt{\overline{x^2}}} \delta^{1/6}.$$

According to the last expression, if the signal is a periodic function $a \cos(\omega t)$, then the output amplitude is

$$A = \sqrt{a}\, \delta^{1/6}. \tag{8}$$

## C. Interacting sensors

In the TH sensor, the positive feedback (a resistor-inductor circuit) passes the oscillating signal component, as well as the dc component [that is proportional to $f(x,q)$], to the primary coil of the magnetic sensor. Hence the magnetic sensor creates

a "self" magnetic field that interferes with the target magnetic field $s$. The magnetic field of the sensor is proportional to $f(x,q)$,

$$\phi(t) \propto f(s + \xi, q).$$

Since the oscillator voltage [proportional to $f(x,q)$] is applied to a resistor-inductor circuit at very low frequency, the impedance of the inductor $L_1$ is very small. Hence the value of the current (and magnetic field) in the $RL_1$ circuit is mainly controlled by the resistor $R$ and is proportional to $\sqrt{q}$.

We begin our treatment of the coupled system by considering two identical sensors separated by the interval $l$,

$$T \frac{d}{dt} \psi_1(t) = -\psi_1(t) + [f(s + \xi_1(t) + \phi_1(t), q_1(t))]^2,$$

$$\tau \frac{dq_1}{dt} q_1(t) = -q_1(t) + \psi_1(t)\delta^{-2/3},$$

$$T \frac{d}{dt} \psi_2(t) = -\psi_2(t) + [f(s + \xi_2(t) + \phi_2(t), q_2(t))]^2, \qquad (9)$$

$$\tau \frac{dq_2}{dt} q_2(t) = -q_2(t) + \psi_2(t)\delta^{-2/3},$$

that interact via their (self-)generated magnetic fields:

$$\phi_1(t) = \frac{g}{l^3}\sqrt{\hat{q}_2} f(s + \hat{\xi}_2 + \hat{\phi}_2, \hat{q}_2),$$

$$\phi_2(t) = \frac{g}{l^3}\sqrt{\hat{q}_1} f(s + \hat{\xi}_1 + \hat{\phi}_1, \hat{q}_1). \qquad (10)$$

In Eq. (10) the following parameters are introduced: $\hat{\xi}_1 = \xi_1(t - r)$, $\hat{\phi}_1 = \phi_1(t - r)$, and $\hat{q}_1 = q_1(t - r)$; we note that the parameter $r = l/c$ is the time delay, where $c$ is the speed of light and $g$ the coupling strength.

The system of delay differential equations (2), (9), and (10) has the small parameter $r$. In this case, we may approximate [14] the delay term in the equations with the following ordinary differential terms:

$$\phi_i(\hat{t} + r) \simeq \phi_i(\hat{t}) + r\dot{\phi}_i(\hat{t}), \qquad (11)$$

where the new time, $\hat{t} = t - r$, has been introduced. From this we have

$$r \frac{d}{dt} \phi_1 = -\phi_1 + \frac{g}{l^3}\sqrt{q_2} f(s + \xi_2 + \phi_2, q_2),$$

$$r \frac{d}{dt} \phi_2 = -\phi_2 + \frac{g}{l^3}\sqrt{q_1} f(s + \xi_1 + \phi_1, q_1), \qquad (12)$$

i.e., the model of two coupled sensors has been reduced to the system of ordinary differential equations that can be easily solved numerically. Since we have assumed $r \ll 1$, in many cases the dynamics of the variables $\phi_i$ can be approximated by the equations

$$\phi_1 \simeq \frac{g}{l^3}\sqrt{q_2} f(s + \xi_2 + \phi_2, q_2),$$

$$\phi_2 \simeq \frac{g}{l^3}\sqrt{q_1} f(s + \xi_1 + \phi_1, q_1),$$

i.e., the dynamics are, in essence, independent of the small parameter $r$. Therefore, for simplicity, we retain a fixed value of the parameter $r$ in all our calculations.
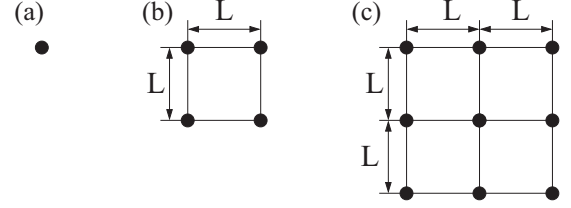


FIG. 6. Organization of the 2D sensory arrays: (a) a single sensor, $N = 1$; (b) $N = 4$ and (c) $N = 9$. The dots denote locations of the sensory units. The parameter $L$ is the intersensor interval.

For a large number of sensors, Eqs. (9) and (12) take on the following forms:

$$z_i = f(s + \xi_i(t) + \phi_i, q_i), \qquad (13)$$

$$T \frac{d}{dt} \psi_i = -\psi_i + z_i^2, \qquad (14)$$

$$\tau \frac{d}{dt} q_i = -q_i + \psi_i(t)\delta^{-2/3}, \qquad (15)$$

$$r \frac{d}{dt} \phi_i = -\phi_i + \sum_{i=1, i \neq j}^{N} \alpha_{i,j} \sqrt{q_j} z_j, \qquad (16)$$

where $i = 1, 2, \ldots, N$. Here it is assumed $r \ll 1$, and $\alpha_{i,j} = g/l_{i,j}^3$, the parameter $l_{i,j}$ is a distance between the sensors $i$ and $j$. In Eq. (16), the dependence of the small parameter $r$ on $l_{i,j}$ is ignored because it is assumed

$$\phi_i \simeq \sum_{j=1, i \neq j}^{N} \alpha_{i,j} \sqrt{q_j} z_j. \qquad (17)$$

The output of the array is $Z = \sum_{j=1}^{N} f(s + \xi_j + \phi_j, q_j)$.

In this study, we will consider sensory arrays organized into square lattices as shown, for example, in Fig. 6. Before moving on, however, it is useful to provide some physical detail regarding how we envision the setup of the array in an experimental system. We assume that each TH sensor is positioned inside its individual Faraday cage made of nonmagnetic material (e.g., copper, aluminium). The cages are *de facto* low pass filters for electromagnetic fields, and can, significantly, reduce the interaction strength between TH elements at their natural frequencies. At low frequency, however, the Faraday cages lose their effectiveness, so that the sensors are affected by the target magnetic field (this field is dc or at very low frequency) and the quasistatic parasitic magnetic fields from neighboring sensors, as well as the low frequency components of the noise.

## III. SIGNAL-TO-NOISE RATIO

The design of the sensor with the tuning feedback leads to the independence of the output of the sensor when the signal is truly constant (which in practice is never the case). Therefore, we actually observe a target field $s$ that is time dependent. To characterize the performance of the system we now estimate the signal-to-noise ratio at the output of the array.

For a periodic signal $a \cos(\Omega t)$ at the input, the output of the sensor, $z$, contains a periodic component $A \cos(\Omega t + \theta)$.

Computer simulations show that the phase $\theta$ is close to zero for a broad range of parameters of the system. Therefore, we may ignore it and assume the output to be $A \cos(\Omega t)$.

The amplitude $A$ can be found via the Fourier transform,

$$A = \frac{2}{T_p} \int_0^{T_p} z(t) \cos(\Omega t) dt,$$

where $T_p = 2\pi/\Omega$. Since $s(t)/a = \cos(\Omega t)$, the last expression can be rewritten as

$$A = \frac{2}{T_p} \frac{1}{a} \int_0^{T_p} z(t) s(t) dt,$$

or

$$A = \lim_{t_2 - t_1 \to \infty} \frac{2}{t_2 - t_1} \frac{1}{a} \int_{t_1}^{t_2} z(t) s(t) dt = \frac{2}{a} \overline{z(t) s(t)}.$$

The total power at the output is $\overline{z^2}$. The power in the periodic component in the output is $P_s = A^2/2$. Thus the noise power is $P_n = \overline{z^2} - P_s$. Now, we can introduce the signal-to-noise ratio,

$$\Gamma = \frac{P_s}{P_n} = \frac{\dfrac{A^2}{2}}{\overline{z^2} - \dfrac{A^2}{2}} = \frac{\dfrac{A^2}{2\overline{z^2}}}{1 - \dfrac{A^2}{2\overline{z^2}}}.$$

Here,

$$\frac{A^2}{2\overline{z^2}} = \frac{[\overline{z(t) s(t)}]^2}{\dfrac{a^2}{2} \, \overline{z^2}}.$$

Assuming $\overline{z} = 0$ and $\overline{s} = 0$, we can rewrite the last expression as

$$\frac{A^2}{2\overline{z^2}} = \frac{[\overline{z\,s} - \overline{z}\,\overline{s}]^2}{(\overline{s^2} - [\overline{s}]^2)\,(\overline{z^2} - [\overline{z}]^2)} = C^2.$$

Here, we have introduced the coefficient $C$ that bears the hallmarks of a correlation coefficient (see next paragraph). In terms of $C$, we can write down the SNR as

$$\Gamma = \frac{C^2}{1 - C^2}. \tag{18}$$

We note that the coefficient $C$ describes the statistical dependence of the output of the array $Z$ on the target field $s$,

$$C = \frac{\overline{Z\,s} - \overline{Z}\,\overline{s}}{\sigma_Z \sigma_s}, \tag{19}$$

where $\sigma_Z^2 = \overline{Z^2} - (\overline{Z})^2$, $\sigma_s^2 = \overline{s^2} - (\overline{s})^2$, and the overline denotes the time averaging, $\overline{s} = (t_2 - t_1)^{-1} \int_{t_1}^{t_2} s\, dt$ and $\overline{s^2} = (t_2 - t_1)^{-1} \int_{t_1}^{t_2} s^2\, dt$. Here we have assumed that $(t_2 - t_1) \to \infty$. The structure of Eq. (19) is similar to a correlation coefficient. Indeed, the difference arises through the form of the averaging: time averaging is used in Eq. (19), and ensemble averaging is used in the correlation coefficient. Therefore, Eq. (19) and the correlation coefficient could, in general, yield different results (due to the difference in averaging) when $s$ is nonstationary.

Before considering the form of the RE in this system, it is necessary to compute an ideal (or theoretical) limit for the net SNR resulting from an uncoupled array (meaning the separation $L$ becomes extremely large) of identical sensors. With only a single sensor, and a very weak periodic signal $s = a \, \sin(\Omega t)$, we can use a linear approximation, $Z_1 = k_q(s + \xi)$, for the transfer function. According to Eq. (19) the coefficient $C$ is

$$C_1^2 = \frac{k_q^2 \dfrac{a^4}{4}}{k_q^2 \dfrac{a^2}{2} \left( \dfrac{a^2}{2} + \sigma_\xi^2 \right)} = \frac{\dfrac{a^2}{2}}{\dfrac{a^2}{2} + \sigma_\xi^2}. \tag{20}$$

The signal-to-noise ratio can then be rewritten as

$$\Gamma_1 = \frac{a^2/2}{\sigma_\xi^2}. \tag{21}$$

The output of an array of $N$ sensors for a weak periodic signal can be written, in the linear approximation, as

$$Z_N = k_q \left( Ns + \sum_{i=1}^{N} \xi_i \right).$$

The coefficient $C$ takes on the form

$$C_N^2 = \frac{\dfrac{a^2}{2}}{\dfrac{a^2}{2} + \dfrac{\sigma_\xi^2}{N}}, \tag{22}$$

where we assume a statistical independence of the noises $\xi_i$.

From Eq. (21) and Eq. (22) it follows that

$$\Gamma_N = N\,\Gamma_1. \tag{23}$$

This allows us to predict a theoretical dependence of the signal-to-noise ratio for an array with $N$ units if $\Gamma_1$ is known, for the "ideal" case of widely separated sensors (i.e., the coupling is negligible).

## IV. RESULTS AND DISCUSSION

Figure 7 shows that, in the case of a weak periodic signal, the performance of the sensory system is better when the intersensor intervals are longer (weak coupling). It is easy to see that the obtained results are always below the capacity defined as the theoretical dependence.

If the periodic signal is strong (see Fig. 8), the dependence of the SNR on the intersensor spacing is also strong. One readily finds that the amplitude of the output increases with the amplitude of the input signal [see Eq. (8)]. This means that the increased amplitude of the input signal leads to an increase in the magnetic field created by the sensor and, hence, to an increased strength of the interactions between the sensors. Every sensor in the array amplifies both the target signal and the magnetic field of other sensors of the array. The unwanted positive feedback stemming from coupling between the sensors "confuses" their tuning mechanisms so that the amplitude $A$ of the array output is greater than expected (see Fig. 9), and the magnitude of the inputs of the sensors can be outside the working dynamic range. Therefore, the
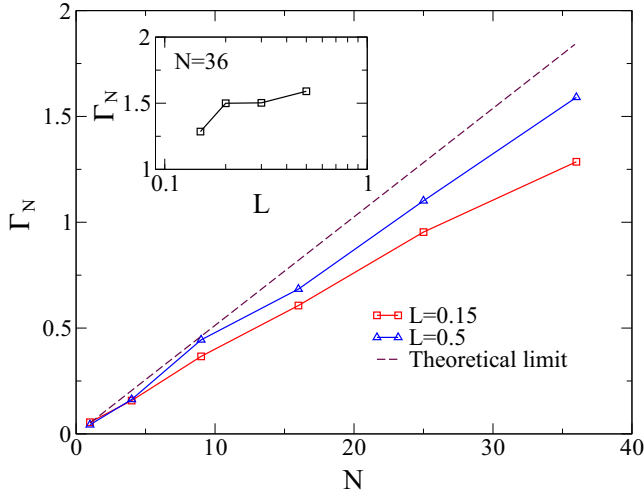
FIG. 7. Ringelmann effect in an array of sensors. The signal-to-noise ratio $\Gamma_N$ as a function of the number $N$ of sensors in the array. The array is organized into the square lattices (see Fig. 6) with the intersensor intervals $L$. The target field is the weak periodic signal $x = a \sin(\Omega t)$, where $a = 0.001$ and $\Omega = 2\pi \times 0.01$. The noises $\xi_i(t)$ are independent OU stochastic processes. The theoretical dependence is shown with the dashed line. It was found with Eq. (23). It is easy to see that the obtained results are always below the theoretical capacity. This is a sign of the Ringelmann effect in our coupled array. The inset shows a clear increase in the summed SNR response (for fixed $N = 36$) as the sensor separation in the array increases, corresponding to a lower coupling strength.

sensors become nonlinear systems that pass the signal with a nonlinear distortion. From the SNR definition Eq. (18), the higher harmonics of the signal make a contribution to the noise in the outputs of the sensors, so that the SNR is reduced. It is easy to see that

$$\Gamma_{\text{actual}} < \Gamma_{\text{expected}} \equiv \sum_{i=1}^{N} \Gamma_{i,\text{alone}}, \quad i = 1 \ldots N. \qquad (24)$$
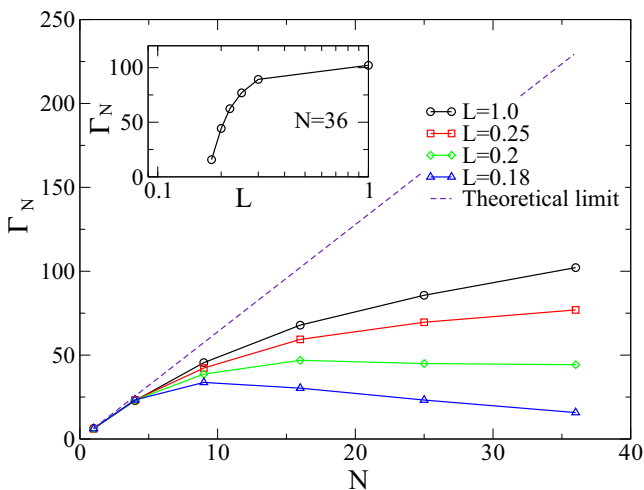


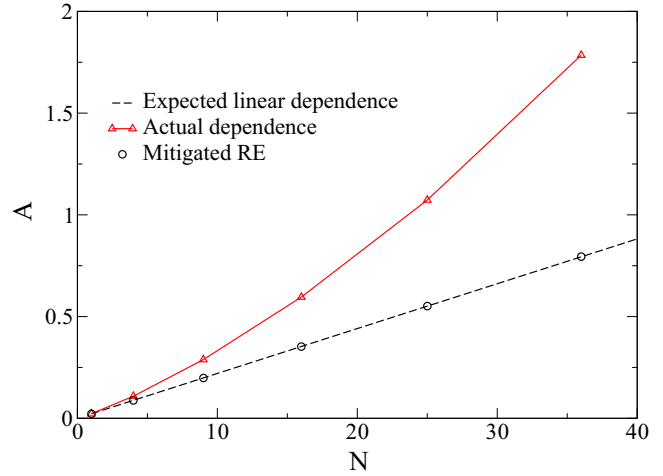FIG. 8. Ringelmann effect in an array of sensors. Same parameters as Fig. 7 but with $a = 0.01$.



FIG. 9. Synergetic effect of the coupling on the gain in the array. Here $A$ is the output amplitude of the array. The periodic input signal is $x = a \cos \Omega t$. Parameters: $\Omega = 2\pi \times 0.01$, $a = 0.01$, $\delta = 0.01$, $T = \tau = 10$, and $L = 0.18$. The expected theoretical dependence was obtained with Eq. (8) and assumption that the amplitude is $A = N \times A_0$, where $A_0$ is the amplitude of the unit (of the array) performing alone.

Comparing Eq. (1) and Eq. (24), we conclude that the inequality Eq. (24) satisfies the definition of the RE, with the one caveat: instead of the maximal productivity, we use the SNR in the system as a performance measure. The SNR is almost the same whether the sensor is optimally tuned or not, as long as the input $x$ of the transfer function $f(x,q)$ is within the dynamic range. Hence the maximum SNR is equivalent to the optimal SNR. Therefore, we may use the term "Ringelmann effect" in the context of the reduction of the SNR in the array of sensors.

In contrast to Fig. 7, Fig. 8 shows that the SNR is a nonmonotonic function of the number of the units in the array. In fact, there arises a situation wherein the number of mutual interactions grows faster than the number of units in the array. Every interaction makes its individual contribution to the positive feedback of the system and increases strength of the interactions.

Figure 8 (inset) shows that the reduction of the inter-sensor intervals $L$ (meaning an increase in the coupling strength) leads to a reduction of the performance of the sensory system, i.e., the SNR rapidly drops. Obviously, there is a critical $L$ that corresponds to a transition of the system behavior from the amplification of the external magnetic fields to the generation of a spontaneous magnetic field magnetization) that is mostly independent of external fields. This phenomena is similar to a phase transition [15]. An analogous effect is apparent as a function of $N$ (see Fig. 8). For strong coupling (small separation $L$), the "self" fields (arising from the spontaneous magnetization of the core) of each sensor are amplified far more than the external magnetic field. In the large $L$ (i.e., weak coupling) limit the response approaches the theoretical maximum, particularly for weak target signals. These two regimes are, loosely, connected via a maximum in the $SNR$ versus $N$ curve as visible in Fig. 8. As $N$ decreases, the maximum shifts to a lower $N$ value.

To illustrate the influence of the coupling on the sensory system we consider a square matrix consisting of sensor elements that have the individual SNRs,

$$\Gamma_{m,n} = \frac{c_{m,n}^2}{1 - c_{m,n}^2},\qquad (25)$$

where the coefficients $c_{m,n}$ are

$$c_{m,n} = \frac{\overline{z_{m,n}\,s} - \overline{z_{m,n}}\,\overline{s}}{\sigma_{z_{m,n}}\sigma_s},$$

$z_{m,n} = f(s + \xi_{m,n}, q_{m,n})$, $m = 1,\dots,\sqrt{N}$, and $n = 1,\dots,\sqrt{N}$.

We now consider the (numerical) results for the almost independent sensors, i.e., the sensors are weakly coupled due to the long intersensor intervals (we take $L = 1$ for this case). It is easy to see that the individual signal-to-noise ratios $\Gamma_{m,n}$ in all matrices are almost identical and close to value of the SNR of the single sensor ($N = 1$). We illustrate this by using a strong signal (amplitude $a = 0.01$) and computing, for a single sensor, $\Gamma_1 = 6.326391$. For a 2D square lattice of varying size, we can calculate the individual signal-to-noise ratios $\Gamma_{m,n}$ as follows.

$N = 4$:

$$\begin{pmatrix} 6.159971 & 6.433196 \\ 6.456477 & 6.349792 \end{pmatrix}. \qquad (26)$$

Total $\Gamma_4$ is 22.818512.

$N = 9$:

$$\begin{pmatrix} 6.297275 & 6.458169 & 6.403746 \\ 6.374942 & 6.431465 & 6.333464 \\ 6.556485 & 6.643418 & 6.327900 \end{pmatrix}. \qquad (27)$$

Total $\Gamma_9$ is 45.484923, and so on. It is easy to see that the total SNR is less than the sum of all SNRs, i.e., much redundant information passes through the sensory system.

Another illustrative example can be considered, wherein the coupling is strong due to the short inter-sensor intervals, $L = 0.18$. As in the preceding case we can calculate $\Gamma_1 = 6.234534$ for a single element. In this case, we find, as above, the following.

$N = 4$:

$$\begin{pmatrix} 11.158677 & 11.292682 \\ 11.451936 & 11.118461 \end{pmatrix}. \qquad (28)$$

Total $\Gamma_4$ is 23.293699.

$N = 9$:

$$\begin{pmatrix} 14.360633 & 16.886906 & 14.651738 \\ 16.707638 & 19.346849 & 17.575212 \\ 14.750152 & 16.593489 & 15.213220 \end{pmatrix}. \qquad (29)$$

Total $\Gamma_9$ is 33.708725.

The sensors are "cooperating". The individual SNRs are greater than the SNR of the single sensor, and correlations between the individual responses of the sensors and the external signal are increased. But, the cooperative work counters the performance of the whole system; the total SNR is (for increasing $N$) below that of the weakly coupled sensors (the previous case for $L = 1$), with correlations between individual responses being increased in this case.

## V. RINGELMANN EFFECT: SOCIOLOGY MEETS PHYSICS

The coupling-induced phenomena detailed above bear resemblances to the phenomena described by Max Ringelmann 103 years ago [13]; the so-called Ringelmann effect (RE) is frequently cited in the social sciences literature [16,17]. We believe the similarity is much more than a qualitative coincidence and is based on similar dynamical principles mediated by the coupling.

In his studies, Ringelmann focused on the maximum performance of humans involved in experiments wherein they used different methods to push or pull a load horizontally [13]. The RE has already been introduced in Sec. I; here, we provide some more detail. Ringelmann discriminated two main contributions to human productivity losses (see, e.g., Fig. 10), namely the motivation loss (now referred to in the contemporary literature as "social loafing") and a "coordination" loss; he concentrated, however, on the coordination loss as an explanation for the reduction of performance [17]. Ringelmann believed that coordination loss was the more important contributor to the RE because similar reductions in performance occurred not only in groups of humans and animals (horses and oxen [18]), but also in technical systems wherein social loafing was, clearly, impossible. For example, in multicylinder combustion engines, the engines with the larger number of cylinders produced less power per cylinder [13,17].

One hundred years ago it was too difficult to create a mathematical description of the Ringelmann effect (RE) because of a lack of understanding of complex systems. Consequently, the coordination losses observed by Ringelmann have never been explained or understood. In contrast, the performance loss due to social loafing has been well studied by social scientists. They found that social loafing was not limited to
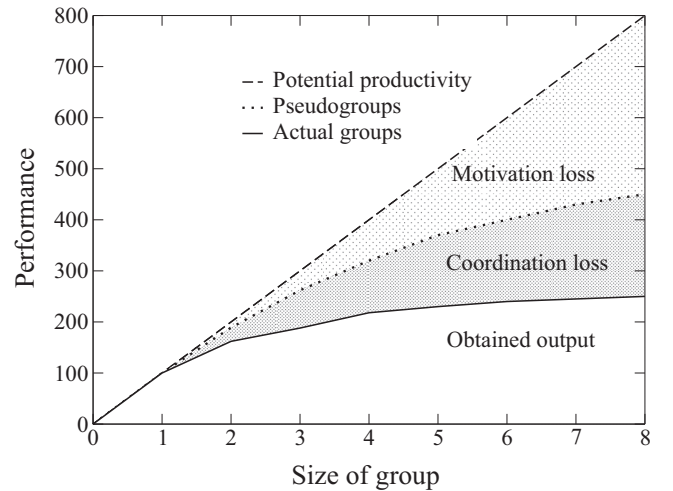


FIG. 10. There are the two major causes of productivity losses in groups working on additive tasks. The portion between the dashed line and the dotted line represents motivation loss (social loafing), and the portion between the dotted line and the solid line represents coordination loss. "Pseudogroups" are defined as groups of individuals who were actually working alone, but thought they were working as part of a group. The design of the figure was adopted from Ref. [16].

groups that needed to exert physical effort. The social loafing could, in fact, be observed when groups worked at diverse tasks, e.g., maze performance [19], evaluating a poem [20], song writing [21], brainstorming [22], reacting to proposals [23], judgmental tasks [24], research [25], software developing [26–28], pumping air [29], clapping [30], rowing [31], pulling a rope [32], swimming in relay races [33], job selection decisions, typing, and creativity problems [16,34].

Social scientists paid far greater attention to the social loafing component of the RE, because it was believed that these studies might provide the framework to organize a team that could improve its performance by increasing individual efforts in groups [16,34]. Today, these studies are motivated by the interest of industrial organizations for achieving an improvement of their efficiency through the most optimal organization.

In this work, we have studied (for a coupled sensor array) another type of contribution to productivity loss; this contribution stems from interactions between members of a group which we believe is also the origin of the coordination loss reported by Ringelmann. To illustrate the interaction-induced loss we start by discussing Ringelmann's original experiments relating to a human horizontally pulling a rope attached to a dynamometer [13]. In the experiments, the subject's feet are in contact with the ground and the body slopes to create tension in the rope with the help of gravity; as the slope and hence pulling force increases so does the balancing frictional force on the ground. For some critical slope the pulling force equals the maximum sustainable frictional force giving rise to a "critical point". Exceeding this slope (force) results in loss of stability. Thus, for the "best" performance, the subject should remain close to the critical point while not going past it (i.e., remain within the "working range"). We can assume that the subject uses the following control "algorithm" to adjust (tune) his body to the critical position. The subject increases his slope until slippage starts to occur; he, then, stumbles backwards to correct the sliding. This process is then repeated with the subject trying to "bias" his position as close to the critical point as possible without slipping. Near the critical point fluctuations are amplified; therefore, the body of the subject moves randomly with multiple corrections required to prevent, or as a consequence of, slippage. If a group of humans are pulling the rope, unintentional random movement of one member will dramatically affect the "tuning" processes of other members of the group. To avoid loss of stability in the presence of common fluctuations, the members of the group will keep the positions of their bodies away from the critical state. Hence the net performance of the humans will be reduced.

In his pulling-the-rope experiments, Ringelmann asked the subjects to maintain a maximum effort for 4–5 s [13]. Given this relatively long duration it is not really conceivable that subjects were unable to pull at the same time, i.e., they would have been able to synchronize their efforts. Consequently, the coordination losses measured by Ringelmann were, almost certainly, caused by the (unintentional) movement of the rope that was fed back to members through the mechanical coupling of the rope itself.

In this paper we have studied a physical system that is not similar to the group of humans in Ringelmann's experiments, but the coupling-induced dynamics does have a similar impact on performance; the coupling channels fluctuations from individual sensor outputs to adjacent sensors which are themselves already optimally tuned (i.e., their dynamic range, and hence SNR, is maximized). The fluctuations therefore perturb the sensors away from their optimal working point thus lowering overall performance.

From an application perspective mitigation of the RE is necessary to enhance performance. We now provide a possible path to mitigating the losses in arrays of nonlinear engineered devices.

### Can the Ringelmann effect be mitigated?

According to Figs. 7 and 8, the RE can be mitigated by increasing the element separation $L$ in the sensory array. But, in this case the size of the array will either become prohibitively large or result in sensors picking up different spatially localized signals. Hence an alternative way of reducing the RE is required.

Since the RE takes place due to the coupling between the sensory units we could, at least on paper, cancel the coupling term $\phi_i$ in Eq. (13) to improve the SNR response of the array. However, in contrast to the mathematical model, the simple "cancellation of the coupling term" is usually impossible in a real sensory system. Therefore, we construct the canceling term $\Phi_{c,i}$ to the coupling term $\phi_i$ in Eq. (13), from data available from measurements in a possible real experiment; ideally, the canceling term should be $\Phi_{c,i} = -\phi_i$. In keeping with our desire to achieve the mitigation of the RE through realistic (i.e., experimentally accessible) scenarios, however, we assume that it is impossible to measure the quantity $\phi_i$. According to Eq. (17), however, this quantity can be estimated from a knowledge of the parameters $g$, $l_{i,j}$, $q_i$, and $z_i$, where $i = 1, \ldots, N$. For simplicity, we will assume that the dynamics of all parameters $q_i$ are similar and all $q_i$ take on almost the same values, $q_i \simeq q_j$. Then the canceling term will be

$$\Phi_{c,i} = -g\sqrt{q_i} \sum_{j=1, i \neq j}^{N} \frac{z_j}{l_{i,j}}, \qquad (30)$$

where $z_j$ is the output of the $j$th unit. Hence Eq. (13) can be rewritten as

$$z_i = f(s + \xi_i(t) + \phi_i + \Phi_{c,i}, q_i). \qquad (31)$$

The term $\Phi_{c,i}$ in Eq. (31) implies a global feedback in the sensory system, as shown in Fig. 11. In Fig. 11(a) the circuit of a single unit of the array with the output $z$ and the additive input $\Phi_c$ is shown. Figure 11(b) shows the global feedback for each unit. The results stemming from the feedbacks can be seen in Fig. 12. The SNR is significantly improved but the theoretical limit is not reached due to the (still) nonideal structure of the canceling term $\Phi_{c,i}$ [see Eq. (30)].

Throughout this paper, the biomimetic nature of the magnetometer array was inspired by what is generally accepted to occur in the auditory system [36,37]. Consequently, our approach raises a number of interesting questions. If the receptors are mechanically coupled via the basilar membrane–tectorial membrane system (see Fig. 13), could the RE occur in the auditory system? If yes, then can the auditory system mitigate the RE? In (the schematic) Fig. 13, we show that the central nervous system not only receives signals from
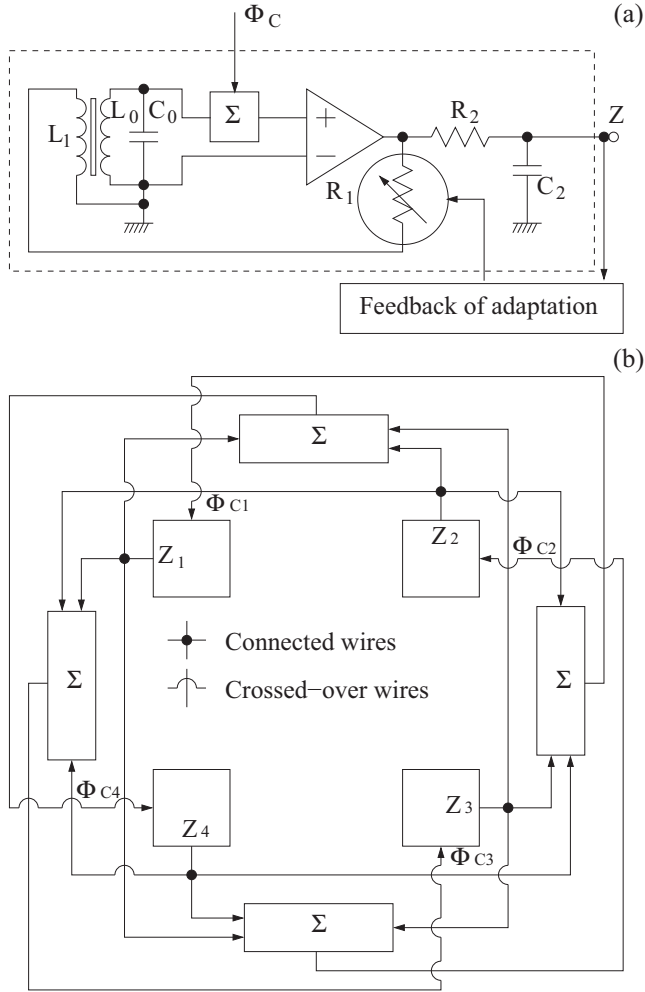
FIG. 11. (a) Circuit of the sensory unit. Since the parameter $q$ should depend on $R_1$, in the figure we show that the variable resistor $R_1$ is a target for the feedback of the adaptation (self-tuning mechanism). (b) The complete system with four units. The blocks marked with $\sum$ are summators with different weights as required by Eq. (30).
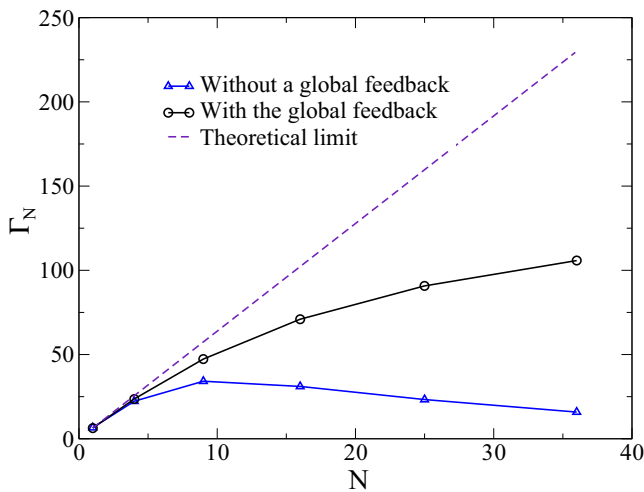


FIG. 12. Mitigating the Ringelmann effect in an array of sensors. Same parameters as Fig. 8 with separation $L = 0.18$.
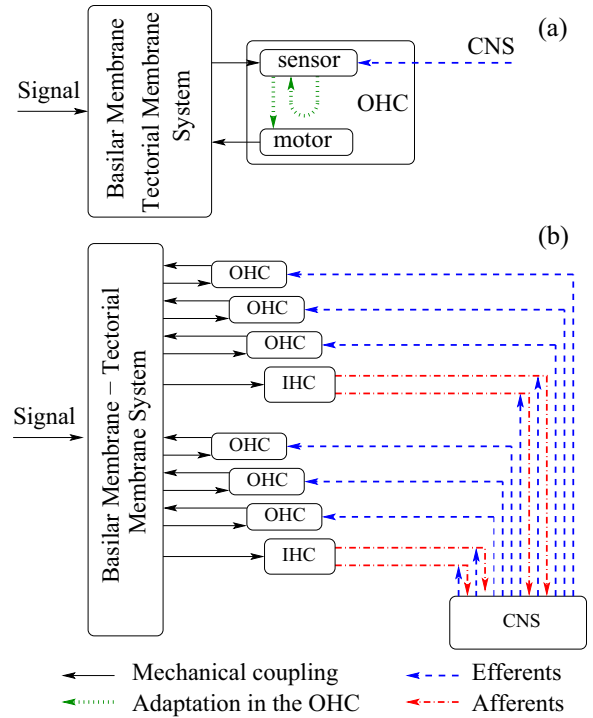


FIG. 13. (a) Outer hair cell (OHC) interacting with the basilar membrane–tectorial membrane system and with the central nervous system (CNS) [35]. The OHC can schematically be split into the sensor and motor components. The dotted green loop shows that the sensory part of the OHC is adaptive subsystem [36]. (b) The coupling in the auditory system of mammals [37]. The afferents are shown with dash-dotted red arrows targeted to the CNS, and the efferents are shown with dashed blue arrows. Mechanical coupling between the OHCs, and inner hair cells (IHCs) and the basilar membrane–tectorial membrane system are shown with solid black arrows.

inner hair cells but tries to control parameters of outer hair cells. We *could* speculate that the feedback circuits, OHCs → IHCs → afferents → CNS → efferents → OHCs, schematized in Fig. 13 could play the role of a RE mitigating system. We stress that Fig. 13 is our rendition of the adaptive amplification process in the cochlear, based on our reading of references [36,37]. This "provocative speculation" on our part might stimulate further investigations into the nonlinear dynamic phenomena that are considered integral to the auditory system.

## VI. CONCLUSIONS

In this work, we have introduced a model of an array of nonlinear interacting sensors. The individual sensors can be tuned to their optimal regimes for the best performance, when uncoupled. However, in the presence of the other sensors, this optimization (in the individual units) is lost because of coupling induced interaction. This is a "coupling" loss that can lead to a reduction in performance of the entire sensory system.

The performance loss is most evident at smaller intersensor intervals (corresponding to higher coupling strength). The overall performance, quantified by a total SNR, is bounded from above by the theoretical (or ideal) limit given by

$N \times \Gamma_{N=1}$ [Eq. (23)]; this value is approached only in the limit wherein the sensors are, effectively, decoupled.

Clearly, it would be a significant improvement if we could mitigate (or reduce) the losses stemming from the RE in a sensory array of the type considered in this work. One possible route to this, via global feedback, has been proposed. Equation (30) derived from the feedbacks depends on both the geometrical parameters of the array (the separation between sensors $l_{i,j}$) and the outputs $z_i$ of the individual units of the array. Note that Eq. (30) is an approximation of the ideal canceling term $\Phi_{c,i} = -\phi_i$ but, in contrast to the ideal cancellation term, it can be realized via the electrical circuit shown in Fig. 11. Since $\Phi_{c,i}$ differs from $-\phi_i$ (as already mentioned above), it is not able to completely cancel the parasitic coupling $\phi_i$ between the individual elements and sensors. Therefore, the theoretical limit of ideal performance cannot be reached in practice (unless the coupling is, identically, zero) and the RE still limits the array performance, albeit in a greatly reduced form.

We note, here, that social and behavioral scientists often find it difficult to quantify the individual performances of working units that contribute to a total (i.e., group) result; specifically, they usually cannot quantify any of the losses depicted in Fig. 10. Thus, in an effort to quantify individual performances in a group effort it is, often, common practice to scale the performance metric that characterizes the overall performance by the number of working units in the group. Applying this reasoning, the individual (in our case, sensor) performances in each coupled array would be obtained by simply computing the overall SNR performance and scaling it by $N$ to yield the individual performances. Hence, unlike the results of the preceding section, all the component elements in each coupled array would have the same SNR response. For example, in the $L = 0.18$ case, we would obtain $\Gamma = 6.23 \, (N = 1), 5.82 \, (N = 4), 3.74 \, (N = 9)$, etc. Clearly, if the social scientists could, separately, quantify the individual performances of elements in their systems, their results might be similar to the results of this article.

At this point it is worth noting that there does in fact exist at least one exception (that we are aware of) in the social sciences literature, wherein the loafing and coordination losses were, separately, quantified. Latane *et al.* [38] carried out an experiment involving clapping and shouting by a group of human subjects. Among the tests, one in particular stands out: participants were asked to shout as loudly as they could when alone, in pairs, in sixes, etc. The subjects were blindfolded and wearing headphones subject to a masking signal; therefore they were unaware of the presence of other subjects. The trials included situations wherein the subjects (still blindfolded and wearing headphones) were led to believe that they were actually part of a group. A novel testing and measurement procedure allowed the researchers to quantify individual performances when the subjects knew they were alone, and when they thought they were in a group. This allowed the researchers to, separately, quantify the loafing and coordination losses in the group performance. The following extract, directly from the abstract of [38], is self-explanatory: "Two experiments found that when asked to perform the physically exerting tasks of clapping and shouting, people exhibit a sizable decrease in individual effort when performing in groups as compared to when they perform alone. This decrease, which we call social loafing, is in addition to losses due to faulty coordination of group efforts".

Other problems in the quantification of human performance could arise when one confronts a heavy-tailed distribution of contributions of individual group members. For example, in an analysis of open source software production, it was reported that the distribution of contributions per software developer was heavy-tailed, meaning the first two statistical moments (mean and variance) were undefined [28]. Due to the difficulty in correctly defining the performance of software developers and due to problems relating to an estimation of this quantity from available data, the authors of two separate papers [26,27] came to opposite conclusions regarding the presence of a Ringelmann effect in the software production process. It is easy to understand that a similar situation could arise in a sensory array when the TH sensors, that are the backbone of this paper, are replaced with different sensors that might be tuned to different critical behavior, e.g., a phase transition [15] or self-organized criticality [39], instead of the Hopf bifurcation. Such sensors could be very sensitive to weak signals but their noise-floor distributions could be heavy-tailed. Clearly, then, if the first and second moments of the noise distributions are not defined then it will be difficult to correctly quantify the signal-to-noise ratio and estimate the performance of the sensory system.

The results of our work hold for any array of nonlinear sensors (and the coupling can have any form) that can be, individually, tuned to a regime wherein their response to a target signal is optimized. Then, the Ringelmann effect appears to provide the underlying thread between the purely social interactions originally examined by Ringelmann and the (quite complex) sensor arrays that are increasingly possible with today's advanced technology. More importantly, the principles of coupling-induced performance loss should be generic to many systems across the physical, biological, engineering, and social sciences. Adaptive (self-tuning) schemes for operating isolated subunits (e.g., people [16], animals [18], optical sensors and systems [40], parallel inverters and converters in power electronics [41], and antenna arrays [42]) close to their optimal operating points can be devised but become less effective when coupled into a complex interacting network. We have demonstrated that, in addition to the local optimization (adaptation), some form of global optimization, e.g., via feedback, can help to mitigate Ringelmann-type effects. These principles are expected to be generic across a wide class of nonlinear dynamic systems.

It seems fitting to conclude this paper with an exclamation point. While the coupling-induced loss and the RE can occur in many coupled nonlinear dynamic systems (see previous paragraph), it is the self-tuning to an optimal point (effectively poised on the threshold of the Andronov-Hopf bifurcation in our case) that is a central feature of signal processing in the cochlea. Thus our sensor array (and, in fact, the single TH sensor as well) is not biomimetic unless we incorporate the self-tuning mechanism in each sensor prior to setting up the array.

[1] W. Bialek, Annu. Rev. Biophys. Biophys. Chem. **16**, 455 (1987).

[2] K.-E. Kaissling, Annu. Rev. Neurosci. **9**, 121 (1986).

[3] T. H. Bullock and F. P. J. Diecke, J. Physiol. **134**, 47 (1956).

[4] M. N. Coleman and D. M. Boyer, Anat. Rec. **295**, 615 (2012).

[5] C. Kőppl, O. Gleich, and G. A. Manley, J. Comp. Physiol., A **171**, 695 (1993).

[6] G. A. Manley and J. A. Clack, in *Evolution of the Vertebrate Auditory System*, edited by G. A. Manley, A. N. Popper, and R. R. Fay (Springer-Verlag, New York, 2004).

[7] G. A. Manley, Proc. Natl. Acad. Sci. USA **97**, 11736 (2000).

[8] P. Dobbins, Bioinspiration Biomimetics **2**, 19 (2007).

[9] J. Stroble, R. Stone, and S. Watkins, Sensor Rev. **29**, 112 (2009).

[10] A. P. Nikitin, N. G. Stocks, and A. R. Bulsara, Phys. Rev. Lett. **109**, 238103 (2012).

[11] S. Takeuchi and K. Harada, IEEE Trans. Magn. **MAG-20**, 1723 (1984).

[12] S. Camalet, T. Duke, F. Julicher, and J. Prost, Proc. Natl. Acad. Sci. USA **97**, 3183 (2000).

[13] M. Ringelmann, Ann. Inst. Natl. Agron., 2e ser. **XII**, 1 (1913).

[14] R. D. Driver, D. W. Sasser, and M. L. Slater, Math. Assoc. Monthly **80**, 990 (1973).

[15] H. E. Stanley, *Introduction to Phase Transitions and Critical Phenomena* (Oxford University Press, Oxford and New York, 1971).

[16] D. R. Forsyth, *Group Dynamics*, 4th ed. (Thomson/Wadsworth, Belmont, CA, 2006).

[17] D. A. Kravitz and B. Martin, J. Person. Soc. Psych. **50**, 936 (1986).

[18] M. Ringelmann, Ann. Inst. Natl. Agron., 2e ser. **VI**, 243 (1907).

[19] J. M. Jackson and K. D. Williams, J. Person. Soc. Psych. **49**, 937 (1985).

[20] R. E. Petty, S. G. Harkins, K. D. Williams, and B. Latane, Person. Soc. Psych. Bull. **3**, 579 (1977).

[21] J. M. Jackson and V. R. Padgett, Person. Soc. Psych. Bull. **8**, 672 (1982).

[22] S. G. Harkins and R. E. Petty, J. Person. Soc. Psych. **43**, 1214 (1982).

[23] M. A. Brickner, S. G. Harkins, and T. M. Ostrom, J. Person. Soc. Psych. **51**, 763 (1986).

[24] W. Weldon and G. M. Gargano, Organ. Behav. Human Decis. Process. **36**, 348 (1985).

[25] R. Kenna and B. Berche, Res. Eval. **20**, 107 (2011).

[26] D. Sornette, T. Maillart, and G. Ghezzi, PLoS ONE **9**, e103023 (2014).

[27] I. Scholtes, P. Mavrodiev, and F. Schweitzer, Empir. Software Eng. **21**, 642 (2016).

[28] T. Maillart and D. Sornette, arXiv:1608.03608.

[29] N. L. Kerr and S. E. Bruun, Person. Soc. Psych. Bull. **7**, 224 (1981).

[30] S. G. Harkins, B. Latane, and K. Williams, J. Exp. Soc. Psych. **16**, 457 (1980).

[31] C. J. Hardy and R. K. Crace, J. Sport Exercize Psych. **13**, 372 (1991).

[32] A. G. Ingham, G. Levinger, J. Graves, and Y. Peckham, J. Exp. Soc. Psych. **10**, 371 (1974).

[33] K. D. Williams, S. A. Nida, and B. Latane, Basic Appl. Soc. Psych. **10**, 73 (1989).

[34] J. A. Shepperd, Psych. Bull. **113**, 67 (1993).

[35] P. Dallos, J. Neurosci. **12**, 4575 (1992).

[36] R. Fettiplace and C. M. Hackney, Nat. Rev. Neurosci. **7**, 19 (2006).

[37] H. Spoendlin, Am. J. Otolaryngol. **6**, 453 (1985).

[38] B. Latane, K. Williams, and S. Harkins, J. Person. Soc. Psych. **37**, 822 (1979).

[39] P. Bak, C. Tang, and K. Wiesenfeld, Phys. Rev. Lett. **59**, 381 (1987).

[40] J. M. Beckers, Annu. Rev. Astron. Astrophys. **31**, 13 (1993).

[41] N. Hur and K. Nam, IEEE Trans. Ind. Electron. **47**, 871 (2000).

[42] R. L. Yadava, *Antenna and Wave Propagation* (Prentice-Hall of India, New Delhi, India, 2011).